

Active phase and amplitude fluctuations of flagellar beating (accepted for publication in Physical Review Letters)

Rui Ma,^{1,2} Gary S. Klindt,¹ Ingmar H. Riedel-Kruse,³ Frank Jülicher,¹ and Benjamin M. Friedrich¹

¹*Max Planck Institute for the Physics of Complex Systems, Dresden, Germany*

²*Institute for Advanced Study, Tsinghua University, Beijing, China*

³*Department of Bioengineering, Stanford University, Stanford, CA, USA*

(Dated: May 26, 2022)

The eukaryotic flagellum beats periodically, driven by the oscillatory dynamics of molecular motors, to propel cells and pump fluids. Small, but perceivable fluctuations in the beat of individual flagella have physiological implications for synchronization in collections of flagella as well as for hydrodynamic interactions between flagellated swimmers. Here, we characterize phase and amplitude fluctuations of flagellar bending waves using shape mode analysis and limit-cycle reconstruction. We report a quality factor of flagellar oscillations, $Q = 38.0 \pm 16.7$ (mean \pm s.e.). Our analysis shows that flagellar fluctuations are dominantly of active origin. Using a minimal model of collective motor oscillations, we demonstrate how the stochastic dynamics of individual motors can give rise to active small-number fluctuations in motor-cytoskeleton systems.

PACS numbers: 87.18.Tt, 47.63.Gd, 05.40.Ca

Keywords: flagellum, shape mode analysis, Hopf normal form, noise

Systems far from equilibrium such as living matter display active, non-thermal fluctuations, as well as directed motion and oscillations, which are important for biological function. As a prominent example, molecular motors coupled to cytoskeletal filaments convert chemical energy into work and heat to generate motion at the cellular scale. Motor-filament systems can drive mechanical oscillations including spontaneous hair bundles oscillations in the ear [1], mitotic spindle oscillations during cell division [2], sarcomere oscillations in insect flight muscle [3], and the regular bending waves of cilia and flagella, which propel cells in a liquid including sperm and green algae [4], as well as clear mucus in mammalian airways [5]. Cilia and flagella are slender cell appendages of 10–100 μm length, ubiquitously found in non-bacterial cells, which comprise a conversed cylindrical scaffold of microtubules interspersed by dynein molecular motors.

The collective dynamics of the motors working against a visco-elastic load drives flagellar oscillations via a dynamic instability [6]. Force generation by individual motors relies on the stochastic progression through a mechanico-chemical cycle [7]. The stochastic nature of force generation should manifest itself in oscillations that display a characteristic level of noise, representative of active fluctuations. Intriguingly, previous work reported Fourier peaks of finite width in power spectra of flagellar oscillations [8], and phase-slips in pairs of synchronized flagella [9–11], which allowed an indirect assessment of flagellar noise. A direct measurement of flagellar fluctuations is pending, let alone a mechanistic understanding. Flagellar fluctuations impart on biological function: Phase fluctuations of flagellar beating should counter-act synchronization in collections of flagella, which is important for fast swimming [12] and efficient fluid pumping [13]. Amplitude fluctuations will result in noisy swim-

ming paths of flagellated swimmers and impart on hydrodynamic interactions between swimmers [14].

Here, we report direct measurements of phase and amplitude fluctuations of the flagellar beat and discuss the microscopic origin of active flagellar fluctuations using a minimal model. We further illustrate the impact of flagellar fluctuations on swimming and synchronization. Our analysis contributes to a recent interest in driven, out-of-equilibrium systems and their fluctuation fingerprint [15–18] by characterizing noisy limit-cycle dynamics in an ubiquitous motility system, the flagellum.

Flagellar shape analysis. We characterize flagellar beat patterns as superposition of principal shape modes. This dimensionality reduction is key to our fluctuation analysis. We analyze planar beat patterns of bull sperm swimming close to a boundary surface [19], filmed at 250 frames-per-second (corresponding to about 8 frames per beat cycle). The flagellar centerline $\mathbf{r}(s, t)$, tracked as function of arclength position s and time t , can be expressed with respect to a material frame of the sperm head in terms of a tangent angle $\psi(s, t)$

$$\mathbf{r}(s, t) = \mathbf{r}_h(t) - \int_0^s ds' [\cos \psi(s', t) \mathbf{e}_1 + \sin \psi(s', t) \mathbf{e}_2]. \quad (1)$$

Here, $\mathbf{r}_h(t)$ denotes the sperm head center, and \mathbf{e}_1 and \mathbf{e}_2 are ortho-normal vectors with \mathbf{e}_1 pointing along the long head axis, see Fig. 1A. A space-time plot of $\psi(s, t)$ reveals the periodicity of the flagellar beat, see Fig. 1B. This high-dimensional data set can be projected on a low dimensional ‘shape space’ using shape mode analysis based on principal component analysis [20]. The time-averaged tangent angle $\psi_0(s) = \sum_{i=1}^n \psi(s, t_i) / n$ characterizes the mean shape of the beating flagellum ($n=1024$ frames in each movie). We further define a two-point correlation matrix

$M(s, s') = \sum_i [\psi(s, t_i) - \psi_0(s)][\psi(s', t_i) - \psi_0(s')]$, where s, s' range over m equidistant arc-length positions along the flagellum. The eigenvectors $\psi_j(s)$ of the symmetric $m \times m$ -matrix M , sorted by decreasing magnitude of the corresponding eigenvalues, characterize principal shape modes of the flagellar beat. The first two shape modes account for $95 \pm 1\%$ of the variance of the tangent angle data (all measurements are mean \pm s.e., $n=7$ cells). We project the full data set on a two-dimensional shape-space spanned by these two shape-modes

$$\psi(s, t) \approx \psi_0(s) + \beta_1(t)\psi_1(s) + \beta_2(t)\psi_2(s) \quad (2)$$

with shape-coefficients β_1, β_2 obtained by least-square fit, see Fig. 1C,D. Flagellar beating implies periodic shape changes of the flagellum, and thus noisy oscillations of the shape-coefficients with mean frequency $\omega_0 = 2\pi/T$, where $T = 32.4 \pm 1.9$ ms. Individually, $\beta_1(t)\psi_1(s)$ and $\beta_2(t)\psi_2(s)$ describe standing waves; their combination results in a traveling wave propagating from the base to the tip of the flagellum, thereby facilitating net propulsion.

Limit-cycle reconstruction. The point cloud representing subsequent flagellar shapes in Fig. 1D forms a closed loop. This allows us to define a limit-cycle of noisy flagellar oscillations (red) by fitting a closed curve $(\beta_1(\varphi), \beta_2(\varphi))$, parametrized by a phase φ . The phase parametrization of the limit-cycle is defined such that the mean of the phase speed is independent of φ [21]. Thus, φ slightly differs from the polar angle in the (β_1, β_2) -plane. Next, we assign a unique flagellar phase to each tracked flagellar shape by projecting the corresponding point in the (β_1, β_2) -plane radially onto the limit-cycle. The shape trajectory $(\beta_1(t), \beta_2(t))$ avoids the singular origin, thus the instantaneous phase speed $\dot{\varphi}$ is well-defined.

Phase fluctuations. The phase speed $\dot{\varphi}$ has mean equal to the frequency ω_0 of the beat, but can fluctuate around this mean. Phase speed fluctuations cause a decay of the phase-correlation-function $C(t) = \langle \exp[i\varphi(t_0 + t) - \varphi(t_0)] \rangle$, see Fig. 1E. This decay is insensitive to measurement noise that is uncorrelated from frame to frame. The frame-to-frame phase increments $\Delta\varphi_i = \varphi(t_{i+1}) - \varphi(t_i)$ are approximately normally distributed (Fig. 1F, inset). Further, the correlation time of phase speed fluctuations is on the order of our temporal resolution 4 ms or below, and thus short compared to the time-scale of phase decoherence. We can thus interpret the observed phase decoherence using an idealized model of δ -correlated phase speed fluctuations,

$$\dot{\varphi} = \omega_0 + \zeta, \quad (3)$$

where ζ is Gaussian white noise with $\langle \zeta(t)\zeta(t') \rangle = 2D\delta(t-t')$ and D denotes a phase-diffusion coefficient. In this idealization, $|C(t)| = \exp(-D|t|)$. By fitting an exponential to measured $|C(t)|$, we obtain the phase-diffusion coefficient of sperm flagellar beating, $D = 3.2 \pm 1.9 \text{ s}^{-1}$, see

Fig 1E. An alternative measure for the phase stability of oscillations is the quality factor, $Q = \omega_0/(2D) = 38.0 \pm 16.7$, where ω_0/Q indicates the width at half-maximum of the principal peak in the power spectral density of $\exp[i\varphi(t)]$.

The observed phase fluctuations of the flagellar beat are dominantly of active origin and surpass passive, thermal fluctuations by orders-of-magnitude (as suggested by earlier, indirect measurements [10]): For a simple estimate, we consider a flagellar beat that is constrained to move along the shape limit-cycle with φ as only degree of freedom. The friction force P_φ conjugate to φ comprises hydrodynamic friction $\gamma\dot{\varphi}$ and dissipation within the flagellum. We estimate $\gamma \approx 3 \text{ pN } \mu\text{m s}$ [22, 23]. We thus obtain an upper bound $k_B T / \gamma \approx 0.0015 \text{ s}^{-1}$ for the contribution of thermal fluctuations to phase-diffusion D , which is a thousand-fold smaller than the value measured.

Amplitude fluctuations. We define an instantaneous amplitude of the flagellar beat, $A(t) = |\beta_1(t) + i\beta_2(t)| / \rho_0(\varphi(t))$, normalized by $\rho_0(\varphi) = |\bar{\beta}_1(\varphi) + i\bar{\beta}_2(\varphi)|$. Thus, the complex oscillator variable $Z(t) = A(t)e^{i\varphi(t)}$ maps the shape limit-cycle onto the unit circle. In our data, the amplitude $A(t)$ is approximately normally distributed with $\sigma_A^2 = \langle A(t)^2 \rangle - 1 = 0.0070 \pm 0.0023$ [38]. The autocorrelation function of amplitude fluctuations decays with time-constant $\tau_A = 5.9 \pm 1.8$ ms. Interestingly, we find that phase speed correlates with amplitude squared; the slope $-\omega_1$ of a linear regression gives $\omega_1/\omega_0 = 0.38 \pm 0.10$, see Fig. 1F. Thus, the beating flagellum is represented as a non-isochronous oscillator (with approximate isochrones $\varphi - 2\tau_A\omega_1 \ln A = \text{const}$ [24]). Non-isochrony of non-linear oscillators has been related to synchronization [25, 26].

Noisy normal form. Previous theoretical work described the onset of flagellar oscillations as a supercritical Hopf bifurcation [27] with normal form $(\mu > 0)$ [28]

$$\dot{Z} = i(\omega_c - \omega_1|Z|^2)Z + \mu(\Lambda - |Z|^2)Z + \Xi. \quad (4)$$

In the absence of noise, $\Xi = 0$, as considered originally [27], the complex oscillator variable $Z(t) = A(t)e^{i\varphi(t)}$ exhibits spontaneous oscillations with amplitude $A = \Lambda^{1/2}$ and frequency $\omega_0 = \omega_c - \omega_1\Lambda$ for effective motor activity $\Lambda > 0$. In this case, we may assume $\Lambda = 1$ after a parameter transformation.

To study the role of fluctuations, we add a multiplicative noise term $\Xi = Z(\zeta_A + i\zeta_\varphi)$ with uncorrelated Gaussian white noise variables satisfying $\langle \zeta_j(t)\zeta_k(t') \rangle = 2D_j\delta_{jk}\delta(t-t')$, $j, k \in \{A, \varphi\}$, and use Stratonovich interpretation. This choice represents the simplest phase-invariant noise term with tunable phase and amplitude noise strengths D_φ and D_A [29]. For weak noise, $D_A, D_\varphi \ll \mu\Lambda$, amplitude fluctuations satisfy $\langle A(t_0)A(t_0+t) \rangle - 1 \approx \sigma_A^2 \exp(-|t|/\tau_A)$ with correlation-time $\tau_A = (2\mu\Lambda)^{-1}$ and variance $\sigma_A^2 = D_A\tau_A\Lambda$. Phase fluctuations are colored with effective phase-diffusion coefficient $D = D_\varphi + (\omega_1/\mu)^2 D_A$. Our measurements of active

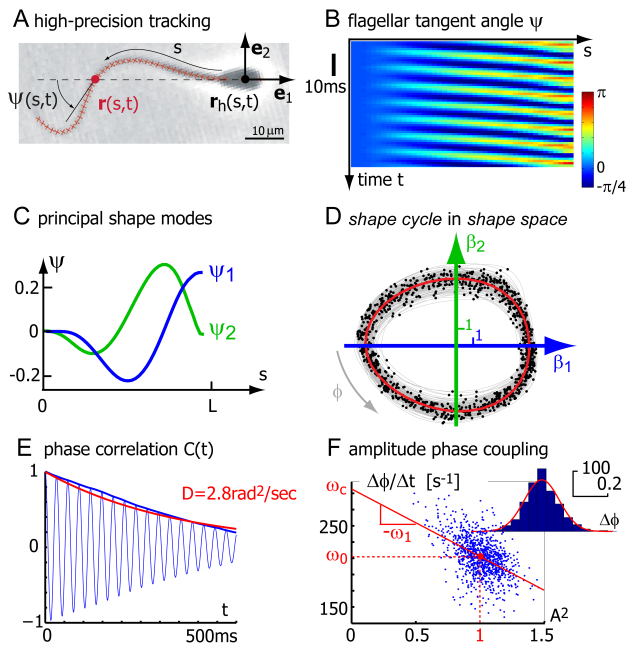


FIG. 1: (color online) The flagellar beat of sperm cells displays active fluctuations. **A**. Tracked flagellar shapes are conveniently characterized by a tangent angle $\psi(s, t)$. **B**. The kymograph of this tangent angle reveals the periodicity of the flagellar beat. **C**. Using principal component analysis, we identify two principal shape-modes $\psi_1(s)$, $\psi_2(s)$, whose superpositions account for 95% of the variability of the tangent angle data. **D**. By projecting the tangent angle data on the shape-space spanned by $\psi_1(s)$ and $\psi_2(s)$, each flagellar shape is assigned a pair of shape-coefficients, (β_1, β_2) , see eq. (2). This representation allows us to define a limit-cycle of perfect periodic beating (red). By projection onto this limit-cycle, we define a phase φ for each flagellar shape. **E**. The flagellar phase-diffusion coefficient D is determined by fitting an exponential decay (red) to the phase correlation function ($|C(t)|$: blue, $\text{Re} C(t)$: light blue). **F**. Phase speed $\Delta\varphi_i/\Delta t$ and squared amplitude $A(t_i)$ are negatively correlated. Inset: phase increments are approximately normally distributed.

flagellar fluctuations thus allow the full parametrization of eq. (4) (with $\Lambda=1$). Note that in the special case $D_A=D_\varphi \ll \mu\Lambda$, our choice of multiplicative noise gives the same long-term behavior as additive noise.

Flagellar fluctuations imply non-deterministic swimming: Using measured noise strengths, we simulated realistic beat patterns and corresponding stochastic swimming paths, see Fig. 3A. Specifically, we (i) use eq. (4) to simulate $Z(t)=A(t)e^{i\varphi(t)}$, (ii) construct shape coefficients $\beta_1(t) + i\beta_2(t) = A(t)\rho_0(\varphi(t))$, and tangent angles $\psi(s, t)$ by eq. (2), (iii) compute the path $\mathbf{r}_h(t)$ using resistive force theory [22] as described in [23]. We find that the center $\mathbf{R}(t)$ of sperm swimming circles diffuses with diffusion coefficient $D_R=3.3 \mu\text{m}^2/\text{s}$, which is on the same order of magnitude, albeit smaller, than a value $D_R=9\pm 2 \mu\text{m}^2/\text{s}$ measured for sea urchin sperm [8]. Our

analysis includes amplitude and phase fluctuations, but neglects additional shape fluctuations; thus our value is a lower bound.

Although phase and amplitude fluctuations are correlated, we can ask separately for their respective effect on swimming. Phase fluctuations cause fluctuations in swimming speed, but do not change the shape of the path. This is because the Stokes equation governing self-propulsion at low Reynolds numbers [30] is invariant under (stochastic) re-parametrizations of time.

To gain qualitative insight into the microscopic origin of noisy oscillations, and the dependence of phase-diffusion on microscopic parameters, we now discuss a minimal motor model and show how it can be mapped onto eq. (4).

A minimal model for noisy motor oscillations. We exemplify how a finite collection of motors drives spontaneous oscillations with characteristic small-number-fluctuations using the classical two-state model [6, 31] in its most simple form: A collection of N motors, rigidly attached to an inextensible backbone interacts with a filament through an effective potential, $W(x)=U[1 - \cos(2\pi x/l)]$, see Fig. 2A. Here x is the coordinate of the motor along the filament, and l the periodicity of the filament. Individual motors can bind to and unbind from the filament with rates $\omega_{\text{on}}(x)=\Omega[\eta - \alpha \cos(2\pi x/l)]$ and $\omega_{\text{off}}=\Omega - \omega_{\text{on}}$. Here, η denotes the mean fraction of attached motors (“duty ratio”). Importantly, the binding rates are spatially inhomogeneous, characterized by α , and break detailed balance. If the filament is now coupled to the backbone by a visco-elastic element with viscosity ξ and elastic stiffness k , we obtain a force-balance equation for the position $X(t)$ of the filament, $kX + \xi\dot{X} = F_m$ with $F_m = -\sum_i \partial_X W(x_i - X)$, where the sum extends over all bound motors and $x_i = il/N$ is a simple choice for the positions of the motors along the backbone.

To properly define a thermodynamic limit for large N , we rescale stiffness and viscosity as $k=k_0N$ and $\xi=\xi_0N$. In the limit $N \rightarrow \infty$, the system can exhibit spontaneous oscillations by a supercritical Hopf-bifurcation, when the normalized motor activity $\xi_a/\xi = 2\pi^2\alpha NU/(\Omega l^2\xi)$ exceeds the threshold $1+\nu$, where $\nu=k/(\xi\Omega)$ [31]. For a finite motor number, we numerically observe noisy oscillations, see Fig. 2.

In the following, we analytically compute the quality factor Q in the limit of large (yet finite) motor number N , assuming that we are close to the Hopf bifurcation with $\varepsilon = \xi_a/\xi - 1 - \nu$ positive and small. Following [31, 32], we first approximated the stochastic binding and unbinding dynamics of individual motors by a diffusion approximation, thus arriving at a Fokker-Planck equation for the probability distribution of filament position and density $\rho(x)$ of bound motors, see appendix for details. Due to the simple choice of potential $W(x)$, the dynamics of the first Fourier mode of $\rho(x)$ decouples from that of the higher modes, resulting in a 3-

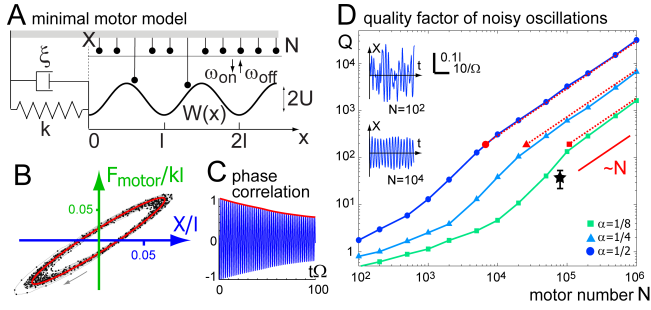


FIG. 2: (color online) A minimal model of coupled motors predicts noisy oscillations. **A.** An ensemble of N motors, grafted at a rigid backbone (gray), can bind and unbind to a filament with transition rates ω_{on} and ω_{off} . Bound motors interact with the filament through an interaction potential $W(x)$. Filament and backbone are coupled visco-elastically. **B.** The motor model exhibits spontaneous, noisy oscillations, here visualized by filament position X and total motor force. The deterministic limit-cycle is shown in red. **C.** The phase correlation function $C(t)$ (real-part shown in blue) decays exponentially, $|C(t)| \approx \exp(-Dt)$, defining the phase-diffusion coefficient D . **D.** The quality factor $Q = \omega_0 / (2D)$ scales with N for large N , consistent with our analytic approximation (dashed red, eq. (5)). The star indicates the experimentally measured Q . For all simulations, we chose parameters close to the Hopf bifurcation ($\xi_a / \xi = 1.2\pi^2$, $\nu = 10$, $\alpha = \eta = 0.5$, $N = 10^4$, unless indicated otherwise; errors smaller than symbol size).

dimensional stochastic system [32]. A non-linear coordinate transformation maps this system onto Hopf normal form eq. (4), with oscillator variable Z satisfying $\text{Re } Z = X/l + \mathcal{O}(\varepsilon^{3/2})$ and phase-dependent noise term $\Xi = i\zeta$, where $\langle \zeta(t)\zeta(t') \rangle = 4D\Lambda\delta(t-t')$. The quality factor $Q = \omega_0 / (2D)$ is found to scale with N

$$Q \approx \frac{\omega_0}{2\Omega} \frac{N\Lambda}{\eta(1-\eta)} \left(\frac{2\pi\alpha}{\sqrt{\nu} + 1/\sqrt{\nu}} \right)^2. \quad (5)$$

Furthermore, $\Lambda \approx \varepsilon(1 + 4\nu) / [3\pi^2\nu(1 + 2\nu)]$, $\mu \approx \Omega\varepsilon / (2\Lambda)$, $\omega_0 \approx \Omega\sqrt{\nu}[1 + \varepsilon / (2 + 4\nu)]$. Interestingly, the motor duty ratio η controls oscillation quality, although η affects neither amplitude nor frequency (for $N \rightarrow \infty$). To understand this, note that the number of bound motors fluctuates with mean ηN and variance $\eta(1-\eta)N$. This number characterizes a spatially homogeneous “background” of bound motors, which does not contribute directly to the oscillations, but sets the amplitude of motor density fluctuations responsible for phase-diffusion. Oscillations become also more regular for increasing amplitude. Eq. (5) and simulations of the full model agree well close to the Hopf bifurcation, see Fig. 2. This minimal motor model recapitulates the experimental observation of phase-diffusion in a minimal setting and illustrates how noisy oscillations can arise from small-number-fluctuations.

Flagellar synchronization. Phase fluctuations cause

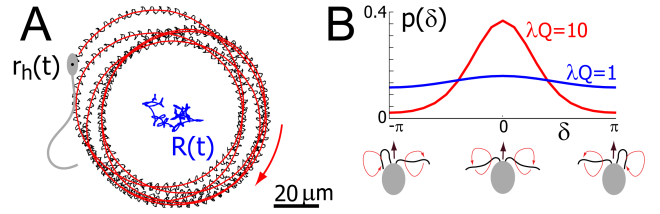


FIG. 3: (color online) Flagellar fluctuations imply non-deterministic swimming and counter-act synchronization. **A.** We simulated stochastic sperm swimming paths $r_h(t)$ (black), using measured flagellar fluctuation strengths. Fluctuations imply that the blue center $R(t)$ of red sperm swimming circles diffuses, with apparent diffusion coefficient $D_R = 3.30 \pm 0.01 \mu\text{m}^2/\text{s}$. **B.** Pairs of flagella can synchronize, e.g. in the green alga *Chlamydomonas*. In a simple description of flagellar synchronization, the phase difference δ between its two flagella peaks around zero for realistic noise strength ($\lambda Q = 10$), but is almost uniformly distributed for ten-fold stronger noise ($\lambda Q = 1$), indicating lack of synchronization.

phase-slips in pairs of synchronized flagella, e.g. in the green algae *Chlamydomonas* [10]. *Chlamydomonas* swims with two flagella, which can synchronize their beat. Analysis of phase-slips allowed a previous, indirect estimate of flagellar phase fluctuations, corresponding to $Q \approx 25$ for the quality factor of individual flagella [10]. A latter study indicated a length-dependence of Q , with corresponding Q ranging from ≈ 70 – 120 for length increasing from $6 \mu\text{m}$ to $12 \mu\text{m}$ [33]. Interestingly, flagellar synchronization in *Chlamydomonas* seems to operate just below a tolerable level of noise: Consider the approximate dynamics of the phase difference δ between two identical, coupled oscillators, $\dot{\delta} = -\lambda/T \sin \delta + \zeta$, where ζ is Gaussian white noise with $\langle \zeta(t)\zeta(t') \rangle = 4D\delta(t-t')$ [10, 34]. Using the estimate $\lambda \approx 0.3$ for the synchronization strength [10], we find $\lambda Q \approx 10$, which yields robust synchronization. A ten-fold higher noise level, however, implies failure of synchronization, see Fig. 3B.

Conclusion. The beating flagellum is a noisy oscillator, driven by $N \approx 8 \cdot 10^4$ dynein motor domains [35]. Here, we precisely measured its phase and amplitude fluctuations, using a novel method of limit-cycle reconstruction [20]. We obtain a quality factor $Q = 38 \pm 16.7$ of flagellar oscillations. Values estimated in other cytoskeletal oscillators are $Q = 2.2 \pm 1.0$ ($N \approx 2500$) for spontaneous hair bundle oscillations [36], and $Q = 1.4 \pm 1.1$ ($N = 10$ – 100) for an *in-vitro* acto-myosin system [16]. We find that the strength of flagellar phase fluctuations is several orders-of-magnitudes above the level corresponding to thermal noise, highlighting the active origin of flagellar fluctuations.

We compute the quality factor Q in a minimal model of motor-filament oscillations, and find that Q is proportional to the number of motors. A simple

numerical example [39] yields noisy oscillations with amplitude, frequency, and quality factor, $Al \approx 68$ nm, $\omega_0 \approx 228$ s $^{-1}$, $Q \approx 33$, which roughly match measured values ($Al \approx 100$ nm, $\omega_0 \approx 200$ s $^{-1}$ [19], $Q \approx 38$). Our analytic approximation eq. (5) is not applicable for these large-amplitude-oscillations. Note that the model does not fully capture flagellar oscillations quantitatively because it strongly simplifies flagellar geometry and motor dynamics.

We show that phase and amplitude fluctuations affect sperm swimming differently: Whereas amplitude fluctuations cause an effective diffusion of sperm swimming circles, phase fluctuations imply speed fluctuations, but do not change the shape of the path. Additionally, phase fluctuations introduce phase-slips in collections of synchronized flagella [10].

Acknowledgments. We thank J Baumgart, VF Geyer, J Howard, P Romanczuk, P Sartori, T Schwalger for stimulating discussions. Experimental data was recorded previously by IH Riedel-Kruse in the laboratory of J Howard.

Our analysis coarse-grains a phase-dependence of flagellar noise, but see [37].

-
- [1] P. Martin, D. Bozovic, Y. Choe, and A. J. Hudspeth, *J Neurosci* **23**, 4533 (2003).
- [2] S. Grill, K. Kruse, and F. Jülicher, *Phys. Rev. Lett.* **94**, 108104 (2005).
- [3] B. Jewell and J. Ruegg, *Proc. Roy. Soc. B* **164**, 428 (1966).
- [4] J. Gray, *Ciliary Movements* (Cambridge Univ. Press, Cambridge, 1928).
- [5] M. J. Sanderson and M. A. Sleight, *J. Cell Sci.* **47**, 331 (1981).
- [6] F. Jülicher and J. Prost, **78**, 4510 (1997).
- [7] J. Howard, *Mechanics of Motor Proteins and the Cytoskeleton* (Sinauer, Sunderland, MA, 2001).
- [8] I. H. Riedel, K. Kruse, and J. Howard, *Science* **309**, 300 (2005).
- [9] M. Polin, I. Tuval, K. Drescher, J. P. Gollub, and R. E. Goldstein, *Science* **325**, 487 (2009).
- [10] R. E. Goldstein, M. Polin, and I. Tuval, *Phys. Rev. Lett.* **103**, 168103 (2009).
- [11] K. Y. Wan, K. C. Leptos, and R. E. Goldstein, pp. 1–12 (2013), arXiv:1312.3673v1.
- [12] C. Brennen and H. Winet, *Ann. Rev. Fluid Mech.* **9**, 339 (1977).
- [13] N. Osterman and A. Vilfan, *Proc. Natl. Acad. Sci. U.S.A.* **108**, 15727 (2011).
- [14] K. Drescher, J. Dunkel, L. H. Cisneros, S. Ganguly, and R. E. Goldstein, *Proc. Natl. Acad. Sci. U.S.A.* **108**, 10940(6) (2011).
- [15] T. Betz, M. Lenz, J.-F. Joanny, and C. Sykes, *Proc. Natl. Acad. Sci. U.S.A.* **106**, 15320 (2009).
- [16] P.-Y. Plaçais, M. Balland, T. Guérin, J.-F. Joanny, and P. Martin, *Phys. Rev. Lett.* **103**, 158102 (2009).
- [17] E. Ben-Isaac, Y. Park, G. Popescu, F. L. H. Brown, N. S. Gov, and Y. Shokef, *Phys. Rev. Lett.* **106**, 238103 (2011).
- [18] M. Otten, A. Nandi, D. Arcizet, M. Gorelashvili, B. Lindner, and D. Heinrich, *Biophys. J.* **102**, 758 (2012).
- [19] I. H. Riedel-Kruse, A. Hilfinger, J. Howard, and F. Jülicher, *HFSP J.* **1**, 192 (2007).
- [20] V. F. Geyer, F. Jülicher, J. Howard, and B. M. Friedrich, *Proc. Natl. Acad. Sci. U.S.A.* **110**, 18058 (2013).
- [21] B. Kralemann, L. Cimponeriu, M. Rosenblum, A. Pikovsky, and R. Mrowka, *Phys. Rev. E* **77**, 066205 (2008).
- [22] J. Gray and G. T. Hancock, *J. exp. Biol.* **32**, 802 (1955).
- [23] B. M. Friedrich, I. H. Riedel-Kruse, J. Howard, and F. Jülicher, *J. exp. Biol.* **213**, 1226 (2010).
- [24] A. Pikovsky, M. Rosenblum, and J. Kurths, *Synchronization* (Cambridge UP, 2001).
- [25] T. Niedermayer, B. Eckhardt, and P. Lenz, *Chaos* **18**, 037128 (2008).
- [26] M. Leoni and T. B. Liverpool, *Phys. Rev. E* **85**, 040901 (2012).
- [27] S. Camalet and F. Jülicher, *New J. Phys.* **2**, 24.1 (2000).
- [28] J. Crawford, *Rev. Mod. Phys.* **63**, 991 (1991).
- [29] R. Graham, *Phys. Rev. A* **25**, 3234 (1982).
- [30] E. Lauga and T. R. Powers, *Rep. Prog. Phys.* **72**, 096601 (2009).
- [31] T. Guérin, J. Prost, and J.-F. Joanny, *EPJE* **34**, 1 (2011).
- [32] T. Guérin, J. Prost, and J.-F. Joanny, *Phys. Rev. E* **84**, 041901 (2011).
- [33] R. E. Goldstein, M. Polin, and I. Tuval, *Phys. Rev. Lett.* **107**, 148103 (2011).
- [34] R. L. Stratonovich, *Topics in the Theory of Random Noise* (Gordon & Breach, 1963).
- [35] D. Nicastro, C. Schwartz, J. Pierson, R. Gaudette, M. E. Porter, and J. R. McIntosh, *Science* **313**, 944 (2006).
- [36] J. Barral, K. Dierkes, B. Lindner, F. Jülicher, and P. Martin, *Proc. Natl. Acad. Sci. U.S.A.* **107**, 10765 (2010).
- [37] K. Y. Wan and R. E. Goldstein, pp. 1–5 (2014), arXiv:1406.3725v1.
- [38] The contribution from measurement noise is small. As a test, we added random perturbations to $\mathbf{r}(s, t)$, using known accuracies of tracking [19]. Phases and amplitudes for perturbed and unperturbed data were strongly correlated; results for σ_A did not significantly change.
- [39] $N=8 \cdot 10^4$, $l=8$ nm, $k \approx 2$ nN/ μ m [7], $\xi \approx 40$ pNs/ μ m, $\Omega=10^4$ s $^{-1}$, $\xi_a/\xi=2$, $\alpha=\eta=0.5$.

Appendix

We present details on the determination of the quality factor of noisy motor-filament oscillations for the minimal motor model discussed in the main text. We first derive a Langevin equation [see Eq. (S16)] for the stochastic motor dynamics using methods presented in [31, 32]. We then show how this Langevin equation can be transformed into a stochastic Hopf normal form using a center manifold technique, see Eq. (S23). From this, we obtain an approximation for the quality factor, see Eq. (S33).

In the minimal motor model [6, 31], a collection of N motors is rigidly connected to a common backbone at equally spaced positions $x_i = il/N$, see Fig. 2A. These motors interact with a filament of periodicity l : Individual motors can bind and unbind from the filament with position-dependent transition rates

$$\omega_{\text{on}}(x) = \Omega[\eta - \alpha \cos(2\pi x/l)], \quad (\text{S1})$$

$$\omega_{\text{off}}(x) = \Omega - \omega_{\text{on}}. \quad (\text{S2})$$

Here, Ω denotes a characteristic transition rate, η the duty ratio of motors, and x a coordinate along the filament, while α characterizes spatial variation of the transition rates. Note that $\omega_{\text{on}}(x) + \omega_{\text{off}}(x) = \Omega$. This so-called uniform rate assumption greatly simplifies the analytical treatment of the model [31]. Motors bound to the filament are subject to an interaction potential

$$W(x) = U[1 - \cos(2\pi x/l)]. \quad (\text{S3})$$

The filament is connected to the motor backbone via an elastic spring of stiffness $k = Nk_0$ and a dashpot with drag coefficient $\xi = N\xi_0$ operating in parallel, see Fig. 2A. The dynamics of the filament is now given by

$$kX + \xi\dot{X} = - \sum_i \partial_X W(x_i - X). \quad (\text{S4})$$

To properly define a thermodynamic limit for large N , we will rescale stiffness and viscosity as $k = k_0N$ and $\xi = \xi_0N$.

Fokker-Planck equation of motor-filament dynamics

We now derive a continuum description for the dynamics of the discrete set of motors. In order to define a probability density $\rho_0(z)$ of bound motors, we divide the interval $[0, l]$ into m bins of width $\Delta = l/m$ and respective bin centers $z_i = i\Delta - \Delta/2$, and set $\rho_0(z_i) = (1/\Delta)n_i/N$, where n_i denotes the number of bound motors within the i -th bin.

Following [32], we can formulate a master equation that governs the evolution of the joint probability distribution $P(X, n_1, \dots, n_m)$ for the filament position X and the bin counts n_i

$$\begin{aligned} \frac{\partial P}{\partial t} = & - \frac{\partial}{\partial X} \left[\left(\sum_{i=1}^m \frac{W'(z_i - X)}{\xi_0} \frac{n_i}{N} - \frac{k_0}{\xi_0} X \right) P \right] \\ & + \sum_{i=1}^m \omega_{\text{off}}(z_i - X) (\mathbf{E}_i^+ - 1) n_i P \\ & + \sum_{i=1}^m \omega_{\text{on}}(z_i - X) (\mathbf{E}_i^- - 1) \left(\frac{N}{m} - n_i \right) P. \end{aligned} \quad (\text{S5})$$

Here, \mathbf{E}_i^\pm denote step operators, whose action on any function $f(n_i)$ obeys $\mathbf{E}_i^\pm f(n_i) = f(n_i \pm 1)$. Using bin center positions as approximate motor positions introduces a relative coarse-graining error $\mathcal{O}(1/m^2)$. To obtain a Fokker-Planck equation for $\rho_0(z)$, we replace $P(X, \{n_i\})$ by $P(X, \rho_0)$, expand Eq. (S5) using the operator expansion

$$\mathbf{E}_i^\pm = 1 \pm \frac{\partial}{\partial n_i} + \frac{1}{2} \frac{\partial^2}{\partial n_i^2} \pm \dots \quad (\text{S6})$$

and neglect all derivatives higher than the second order, which implies a truncation error of order $\mathcal{O}(1/N^2)$, as well as a coarse-graining error of relative order $\mathcal{O}(1/m^2)$. For further simplification, we change the reference frame from the common motor backbone to the co-moving frame of the filament, and use henceforth the density $\rho(x)$ of bound motors with respect to the filament coordinate, $\rho(x) = \rho_0(z - X)$ (where $\rho(x)$ shall be extended outside the interval

$[-X, l - X]$ by periodic continuation for mathematical convenience). This finally leads to a functional Fokker-Planck equation for the distribution function $P(X, \rho)$ (see also [32])

$$\begin{aligned} \frac{\partial P}{\partial t} &= -\frac{\partial}{\partial X} v P + \int_0^l dx \frac{\delta}{\delta \rho(x)} A P \\ &+ \frac{1}{2N} \int_0^l dx \int_0^l dy \delta(x-y) \frac{\delta^2}{\delta \rho(x) \delta \rho(y)} C P. \end{aligned} \quad (S7)$$

The drift terms read

$$v = \int_0^l dx \frac{W'(x)}{\xi_0} \rho(x) - \frac{k_0}{\xi_0} X, \quad (S8)$$

$$A = \omega_{\text{off}}(x) \rho(x) - \omega_{\text{on}}(x) [1/l - \rho(x)] - v \partial_x \rho(x), \quad (S9)$$

while the diffusion term reads

$$C = \omega_{\text{off}}(x) \rho(x) + \omega_{\text{on}}(x) [1/l - \rho(x)]. \quad (S10)$$

Choosing a bin size $m \sim \sqrt{N}$ that increases with the number of motors, we find that both drift terms and diffusion terms in Eq. (S7) are each accurate to leading order in $1/N$.

Spatial Fourier Expansion

We expand $\rho(x)$ into a spatial Fourier series

$$\rho(x) = \frac{\eta}{l} a_0 + \frac{\alpha}{l} \sum_{n=1}^{\infty} a_n \cos\left(2\pi n \frac{x}{l}\right) + b_n \sin\left(2\pi n \frac{x}{l}\right), \quad (S11)$$

and rewrite the functional Fokker-Planck equation (S7) in terms of the Fourier coefficients [32]

$$\begin{aligned} \frac{\partial}{\partial t} P(\{a_n, b_n\}, X, t) &= -\frac{\partial}{\partial X} (v P) - \sum_n \left(\frac{\partial}{\partial a_n} A_n P + \frac{\partial}{\partial b_n} B_n P \right) \\ &+ \sum_{m,n} \frac{\partial^2 D_{mn}^{aa} P}{\partial a_m \partial a_n} + 2 \frac{\partial^2 D_{mn}^{ab} P}{\partial a_m \partial b_n} + \frac{\partial^2 D_{mn}^{bb} P}{\partial b_m \partial b_n}. \end{aligned} \quad (S12)$$

The drift terms A_n, B_n characterize the deterministic mean-field dynamics of the system, and read

$$A_n = \frac{2}{\alpha} \int_0^l A(x) \cos(2\pi n x/l) dx, \quad B_n = \frac{2}{\alpha} \int_0^l A(x) \sin(2\pi n x/l) dx \quad (S13)$$

for $n \geq 1$, while $A_0 = (1/\eta) \int_0^l A(x) dx$ and $B_0 = 0$. The elements of the diffusion matrix characterize the noise effect due to a finite number of motors, and read

$$\begin{aligned} D_{mn}^{aa} &= \frac{2}{N\alpha^2} \int_0^l C(x) \cos(2\pi m x/l) \cos(2\pi n x/l) dx, \\ D_{mn}^{ab} &= \frac{2}{N\alpha^2} \int_0^l C(x) \cos(2\pi m x/l) \sin(2\pi n x/l) dx, \\ D_{mn}^{bb} &= \frac{2}{N\alpha^2} \int_0^l C(x) \sin(2\pi m x/l) \sin(2\pi n x/l) dx. \end{aligned} \quad (S14)$$

In general, the noise strengths are state-dependent. For small oscillation amplitudes and in the limit of weak noise, we can approximate them by their respective values evaluated at the fixed point of the deterministic dynamics, characterized by $a_0 = 1, a_1 = -1, b_1 = 0$. Specifically, we find

$$\begin{aligned} D_a &= D_{11}^{aa} = \frac{\Omega}{2N} \left[\frac{2\eta}{\alpha^2} (1 + a_0(1 - 2\eta)) + 3a_1 \right] \approx \frac{\Omega}{2N} \left[\frac{4\eta(1 - \eta)}{\alpha^2} - 3 \right], \\ D_b &= D_{11}^{bb} = \frac{\Omega}{2N} \left[\frac{2\eta}{\alpha^2} (1 + a_0(1 - 2\eta)) + a_1 \right] \approx \frac{\Omega}{2N} \left[\frac{4\eta(1 - \eta)}{\alpha^2} - 1 \right], \\ D_{11}^{ab} &= \frac{\Omega}{2N} b_1 \approx 0. \end{aligned} \quad (S15)$$

Remarkably, the dynamics of the principal Fourier modes $a = a_1$, $b = b_1$, and filament position X decouples from the other modes [32] with corresponding Langevin dynamics

$$\begin{aligned}\dot{a} &= -\Omega(a + 1 - \gamma b^2 + \beta b X/l) + \zeta_a(t), \\ \dot{b} &= -\Omega(b + \gamma b a - \beta a X/l) + \zeta_b(t), \\ \dot{X} &= \frac{\Omega}{2\pi}(\gamma b - \beta X/l),\end{aligned}\tag{S16}$$

where $\zeta_i(t)$ denote Gaussian white noise terms satisfying $\langle \zeta_i(t)\zeta_j(t') \rangle = 2D_i \delta_{ij}\delta(t-t')$ for $i, j = a, b$, and $\beta/(2\pi) = \nu = k_0/(\xi_0\Omega)$, $\gamma = \xi_a/\xi_0 = 2\pi^2\alpha U/(\Omega l^2\xi_0)$.

We now show how Eq. (S16) can be transformed into Hopf normal form. We first treat the noise-free case, $D_a = D_b = 0$. We first do a linear transformation of the coordinate tuple (a, b, X) to a new set of coordinates, comprising a real variable y and a complex variable Y ,

$$\begin{pmatrix} a + 1 \\ 2b \\ 2X/l \end{pmatrix} = \begin{pmatrix} 1 & 0 & 0 \\ 0 & \chi & \chi^* \\ 0 & 1 & 1 \end{pmatrix} \begin{pmatrix} y \\ Y^* \\ Y \end{pmatrix},\tag{S17}$$

where $\chi = \pi(-\epsilon + 2\nu + 2i\sqrt{\nu})/(\sqrt{\nu} + i)^2$, $\epsilon = \gamma - 1 - \nu$. Conversely, $Y = i(b - \chi X/l)/\text{Im}\chi$ with $\text{Im}\chi = -2\pi/(\sqrt{\nu} + 1/\sqrt{\nu}) + \mathcal{O}(\epsilon)$. In the new coordinate set, the linearized dynamics at the fixed point $(y, Y) = (0, 0)$ is diagonal

$$\frac{d}{dt} \begin{pmatrix} y \\ Y \end{pmatrix} = \begin{pmatrix} -\Omega & 0 \\ 0 & \Omega(\epsilon/2 + i\sqrt{\nu}) \end{pmatrix} \begin{pmatrix} y \\ Y \end{pmatrix}\tag{S18}$$

One can show that y relaxes to an invariant manifold $y = y(Y, Y^*)$ that is tangential to the plane $y = 0$ at $(y, Y) = (0, 0)$. For this so-called center manifold [28], we make a quadratic ansatz

$$y = h_1 Y^2 + h_1^* Y^{*2} + h_2 Y Y^* + \mathcal{O}(|Y|^3)\tag{S19}$$

with complex coefficients h_i that can be determined self-consistently from the full nonlinear dynamics. The dynamics of Y on the manifold defined by (S19) comprises a linear term, as well as cubic terms as leading order nonlinearity

$$\frac{dY}{dt} = \Omega \left(\frac{\epsilon}{2} + i\sqrt{\nu} \right) Y - g_0 Y^3 - g_1 Y^2 Y^* - g_2 Y Y^{*2} - g_3 Y^{*3} + \mathcal{O}(|Y|^4),\tag{S20}$$

where g_i are complex numbers. Using nonlinear coordinate transformations of the form $Y = Z + \theta Z^p Z^{*(3-p)}$, all cubic nonlinearities can be eliminated, with the exception of $Z^2 Z^*$. Thus, we have brought the dynamics of Z into Hopf normal form

$$\frac{dZ}{dt} = \mu(\Lambda - |Z|^2)Z + i(\omega_c - \omega_1|Z|^2)Z + \mathcal{O}(|Z|^4),\tag{S21}$$

with parameters

$$\mu = \frac{3\pi^2\Omega\nu(1+2\nu)}{2(1+4\nu)}, \quad \Lambda = \frac{\Omega\epsilon}{2\mu} = \frac{1}{\pi^2} \frac{\epsilon(1+4\nu)}{3\nu(1+2\nu)}, \quad \omega_c = \Omega\sqrt{\nu}, \quad \omega_1 = -\frac{\mu\sqrt{\nu}}{1+2\nu}.\tag{S22}$$

For $\epsilon > 0$, in the absence of noise, the complex oscillator variable $Z = A \exp i\varphi$ oscillates with amplitude $A = |Z| = \sqrt{\Lambda}$ and frequency $\omega_0 = \omega_c - \omega_1\Lambda$.

In the case of weak noise, we can apply the same series of coordinate transformations used above to the Langevin equation (S16), while neglecting noise-induced drift terms of order $\mathcal{O}(1/N)$

$$\frac{dZ}{dt} = \mu(\Lambda - |Z|^2)Z + i(\omega_c - \omega_1|Z|^2)Z + i\zeta(t),\tag{S23}$$

where $\zeta(t)$ denotes Gaussian white noise with $\langle \zeta(t)\zeta(t') \rangle = 4D_0\Lambda\delta(t-t')$ and noise strength

$$4D_0\Lambda = 2D_b \left(\frac{\sqrt{\nu} + 1/\sqrt{\nu}}{2\pi} \right)^2 + \mathcal{O}(\epsilon).\tag{S24}$$

We now compute the variance of amplitude fluctuations and the phase diffusion coefficient. We consider the limit of weakly perturbed oscillations, $\sigma_A^2 \ll \Lambda$. Using Stratonovich calculus, we derive from Eq. (S23) equations for the instantaneous amplitude A and phase ϕ

$$\dot{A} = \mu(\Lambda - A^2)A + \sin \phi \zeta(t), \quad (\text{S25})$$

$$\dot{\phi} = \omega_c - \omega_1 A^2 + \frac{\cos \phi}{A} \zeta(t). \quad (\text{S26})$$

We approximate the phase-dependent noise strengths by their phase-averaged expectation values, which will reproduce, to leading order in the noise-strength, the same dynamics on time-scales longer than the oscillation period. We also linearize the stochastic dynamics Eq. (S25) for small amplitude fluctuation δA , neglecting terms of order $\mathcal{O}(\delta A^2)$,

$$\frac{d}{dt} \delta A \approx -2\mu\Lambda \delta A + \frac{1}{\sqrt{2}} \zeta(t), \quad (\text{S27})$$

$$\dot{\phi} \approx \omega_c - \omega_1 \Lambda - 2\omega_1 \sqrt{\Lambda} \delta A + \frac{1}{\sqrt{2\Lambda}} \zeta(t). \quad (\text{S28})$$

The first equation describes an Ornstein-Uhlenbeck process with correlation time $\tau_A = (2\mu\Lambda)^{-1}$ and variance

$$\sigma_A^2 = D_0 \Lambda \tau_A = D_0 / (2\mu). \quad (\text{S29})$$

For the phase-diffusion coefficient, we find

$$D = \lim_{t \rightarrow \infty} \frac{1}{2t} (\langle [\varphi(t) - \varphi(0)]^2 \rangle - \langle [\varphi(t) - \varphi(0)] \rangle^2) \quad (\text{S30})$$

$$= \lim_{t \rightarrow \infty} \frac{1}{2t} \langle \int_0^t \int_0^t dt_1 dt_2 \dot{\varphi}(t_1) \dot{\varphi}(t_2) \rangle - \omega_0^2 \quad (\text{S31})$$

$$= \left[1 + \left(\frac{\omega_1}{\mu} \right)^2 \right] D_0. \quad (\text{S32})$$

We now readily find for the quality factor

$$Q = \frac{\omega_0}{2D} = \Theta \frac{\omega_0}{2\Omega} \frac{N\Lambda}{\eta(1-\eta)} \left(\frac{2\pi\alpha}{\sqrt{\nu} + 1/\sqrt{\nu}} \right)^2 \quad (\text{S33})$$

with prefactor

$$\Theta = \left[1 - \frac{\alpha^2}{4\eta(1-\eta)} \right] \left[1 + \left(\frac{\omega_1}{\mu} \right)^2 \right]. \quad (\text{S34})$$

This prefactor can be shown to vary around 1 within close bounds,

$$3/4 \leq \Theta \leq 9/8, \quad (\text{S35})$$

and has therefore been omitted in the approximation presented in the main text. The proof of inequality (S35) involves $0 \leq \alpha \leq \eta$ and $\alpha \leq (1-\eta)$, as well as $|\omega_1/\mu| = \sqrt{\nu}/(1+2\nu) = 2^{-1/2}/[(2\nu)^{-1/2} + (2\nu)^{1/2}] \leq 2^{-3/2}$.

This approximation is only valid for weakly perturbed oscillations with $\sigma_A^2 \ll \Lambda$; the latter condition can be rephrased as $N \gg 1/\epsilon^2$. We remark that amplitude fluctuations remain finite, even at the Hopf bifurcation, and can be shown to scale as $\sigma_A^2 \sim N^{-1/2}$ for $\epsilon = 0$.